Results in Optics 10 (2023) 100337

Contents lists available at ScienceDirect

Results in Optics

journal homepage: www.sciencedirect.com/journal/results-in-optics

Enhancing optical absorption by reducing the trap states in polymer semiconductor processed for solar cell

Arul Varman Kesavan [a], Muthamizh Selvamani [b], Praveen C. Ramamurthy [c,*]

[a] Department of Physics & Nanotechnology, SRM Institute of Science & Technology, Kattankulathur 603203, Tamil Nadu, India
[b] Department of Physiology, Saveetha Dental College & Hospitals, SIMATS, Chennai 600077, Tamil Nadu, India
[c] Department of Materials Engineering, Indian Institute of Science, Bangalore 560012, India

ARTICLE INFO

Keywords:
Thin film
Conducting polymer
Density of trap states
Solar cells
Bulk heterojunction
Absorption

ABSTRACT

Current-voltage characteristics of an organic solar cells can be tuned by tailoring the active layer material's polymer chain ordering which in turn decides the PV performance. The suppression of exciton recombination, improved charge carrier separation, large carrier diffusion length can be achieved by improving the packing density of the π-π stacking, polymer chain length and chain ordering. The high packing density π-π stacking can be formed through enhancing the percentage of crystallinity of the semiconducting polymer layer. This can be achieved by optimizing the processing parameters. This work gives some insights on the spinning time of active layer (P3HT:$PC_{61}BM$) on the structural, optical and solar cell performance. P3HT:$PC_{61}BM$ crystalline properties were studied through grazing incidence X-ray diffraction (GI-XRD). Optical absorption of the active layer was studied by the UV–visible spectrometer. The trap density of states of the solar cells processed at various active layer spinning condition is evaluated. From the obtained result it is noted that device fabricated with longer spinning time showed higher power conversion efficiency over shorter spinning duration. These changes in the device performance could be due to solvent evaporation kinetics, chain alignment in the polymer thin film. Further, the mechanism of trap states formation based on the active layer processing condition is explained.

1. Introduction

The advancement in engineering and technology always looks for miniaturization and flexibility. In the last two decades, organic electronic undergone drastic improvement towards to commercialization (Liu et al., 2020; Sun et al., 2020). Organic solar cells emerges as an energy harvesting technique with short payback time. In the last three decades polymer solar cells have attracted researchers due to many advantages which are cited in literature elsewhere. The soft matter electronics devices find critical issues due to low charge carrier mobility. The low charge carrier mobility of soft matter materials are due to its localized electronic states and disordered nature of it. The degree of localization/delocalization of electronic states depend on chain alignment, conjugation length, degree of disorder, inter-chain interactions, oxidation level of the conducting polymer. In addition to the structural properties, the molecular level forces such as inter and intra molecular forces plays a role in the charge carrier mobility in these types of materials. Moreover, weak intermolecular interaction hinders the charge carrier mobility (Liu et al., 2020). Due to these reasons the organic semiconductors faces poor mobility values, the mobility for such conjugated organic semiconductors varies from 10^{-6} to 1 $cm^2\ V^{-1}s^{-1}$ (Sun et al., 2020). Basically, organic semiconductors (OSC) have low dielectric constants (ε) approximately 2 to 5. Therefore, electron and hole have a strong Coulombic interaction and results a small exciton called Frenkel exciton. These types of excitation usually same order as unit cell size and the energy of such exciton are 0.2 eV to 1.4 eV. In such kind of low dielectric materials light photon interaction generates Frenkel exciton. Therefore, dissociating Frenkel type exciton is necessary to get high power conversion efficiency in case of the organic solar cell device (i) exciton generation (ii) exciton diffusion (iii) exciton dissociation and (iv) exciton recombination (Zhang et al., 2019). In general, polymer solar cell requires the following properties (i) wide range optical absorption (ii) higher charge carrier mobility and so on. Optical absorption can be improved by synthesizing low band gap polymeric semiconductor (Lu and Yu, 2014; Kesavan et al., 2019), increasing degree of crystallinity of the polymer (Zhang et al., 2019; Nellissery Viswanathan et al., 2022), increasing thickness of the active layer. But increasing active layer thickness will increase series resistance and also. Crystallinity in

* Corresponding author.
E-mail address: praveen@iisc.ac.in (P.C. Ramamurthy).

https://doi.org/10.1016/j.rio.2022.100337
Received 6 October 2022; Received in revised form 28 November 2022; Accepted 4 December 2022
Available online 5 December 2022

the conjugated polymers can be obtained by (i) using co-solvent to fabricate the active layer, where the crystallinity has been improved by rearrangement of polymer chains and by improving conjugation length. Moreover, co-solvent film forming method also increases π-π* stacking between inter chain (Zhang et al., 2019; Lu and Yu, 2014). (ii) thermal annealing of regioregular poly(3-hexylthiophane-2,5-diyl) (rr-P3HT) layer enhances edge-on oriented polymer chains for the optimal temperature and time (Liu et al., 2020; Kesavan et al., 2022). (iii) vapor annealing. Vapour annealing and thermal annealing methods allows polymer chain mobility within the thin film layer. These processes modify the spatial reorganization of the polymer chain and fullerene molecule. Solar cell device performance mainly depends on the active layer deposition condition from its blend solution and post deposition process such as solvent selection, thin film solidification rate, thermal annealing of solidified film, vapor annealing of active layer (Kesavan et al., 2019; Rao et al., 2018). Either pre-deposition process or post deposition process, the ultimate goal is to improve crystallinity in the blends layer and to get the optimum phase separation in P3HT and $PC_{61}BM$. Since, efficiency depends on the exciton life time and diffusion length optimum phase separation. In molecular materials mobility of the charge carriers are strongly depends on density of π-π stacking in the thin film. However, the molecular orderings or packing influences both optical absorption and electronics properties such as mobility, carrier life time. In case of semiconductors polymer optoelectronics applications enhancement in these two properties are required. As the crystalline orderings increases in active layer, optical absorption increases as well the mobility and carrier life time. Polymer semiconductors are amorphous in nature. Optical absorption in polymeric semiconductors are strongly dependent on difference between HOMO-LUMO/bandgap, crystalline domain size or degree of molecular orderness present in active layer. Various transport layer were adopted to improve device performance to serve the purpose of transport properties, device stability, improve the transmittance properties improve (Koo et al., 2018; Kesavan and Ramamurthy, 2017; Kesavan et al., 2017). In this work, active layers were grown at different solidification time and their consequences on the device on the device performance were investigated. The growth induced changes in crystallinity and their influence on device performance were accessed based on crystallinity and disorder induced trap states in the semiconductor layer. In bulk hetero-junction (BHJ) photovoltaics, the phase separation of donor and acceptor should be of the order of nanometer scale. In this work, disorder induced electronic defect states was investigated and the materials properties were correlated with the device performance.Fig. 1..

2. Experimental details: photovoltaics fabrication and characterization

The photovoltaics fabrication process is as follows. The indium tin oxide (Xin yan Technology Limited, China) was cleaned by the standard procedure (labolene soap solution, acetone, IPA) and dried with N_2 gas. The dimension and sheet resistance of the ITO is 1 in. by 1 in. and 20 Ω. sq^{-1}. Then, ITO was ultraviolet-ozone treated for 20 min at room temperature. The poly(3,4-ethylenedioxythiophene) polystyrene sulfonate (PEDOT:PSS from Heraeus Epurio Clevios) was deposited on ITO at 3000 rpm for 60sec and then the layer was annealed at temperature 110 °C/10 min. Annealed samples were transferred into the nitrogen filled glove box. The active layer solution was prepared by dissolving P3HT (Rieke metals, USA) and $PC_{61}BM$ (Nano-C Inc., USA) in the 1:0.8 ratio for the total weight of 40 mg in 1 mL of 1,2-dichlorobenzene. The prepared solution was kept stirring for overnight at 50 °C. The obtained solution was filtered and spin coated over PEDOT:PSS layer at the speed of 1000 rpm for all the samples (30sec, 60sec and 200sec). All the samples were annealed at 140 °C for 15 min inside the glove box. Then, the cathode contact was prepared by evaporating Al at the rate 1 $Åsec^{-1}$ to obtain of 100 nm thickness contact. In this work, the devices are referred as device-A:ITO/PEDOT:PSS/P3HT:$PC_{61}BM$(30sec)/Al, device-B:ITO/PEDOT:PSS/P3HT:$PC_{61}BM$(60sec)/Al and device-C:ITO/PEDOT:PSS/P3HT:$PC_{61}BM$(200sec)/Al. Time 30sec, 60sec and 200sec represents the time allowed for spinning the active layer and layer at 1000 rpm.

The optical absorption characteristics of the active layer were studied by Perkin Elmer Lambda35 UV–Visible spectrometer. The active layer crystallinity was studied by Rigaku diffractometer with X-ray diffractometer. P3HT:$PC_{61}BM$ stacking was studied by Raman spectroscopy. The device electrical characteristics was studied by Keithley 4200SCS. External quantum efficiency (EQE) was measured using Enlitech Quantum efficiency measurement system.

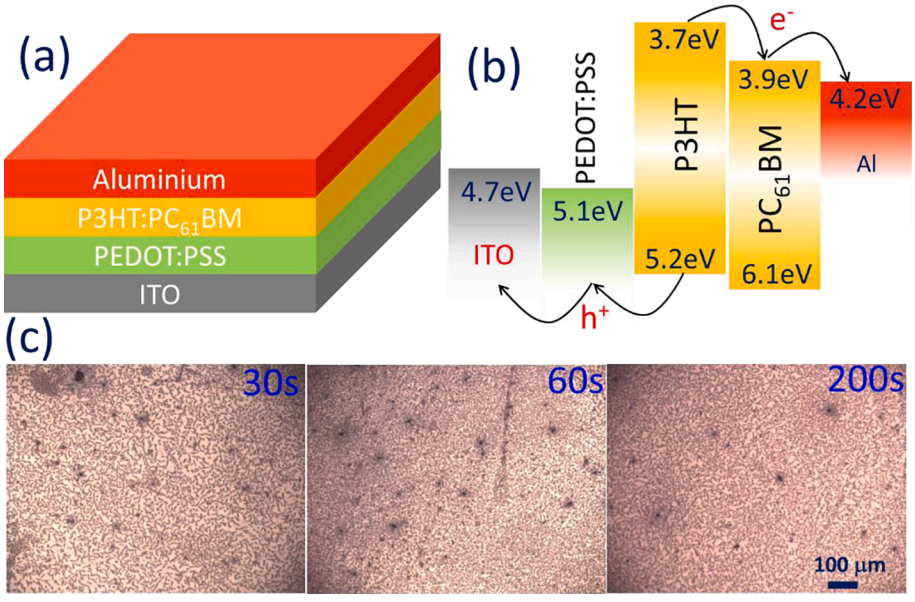

Fig. 1. (a) Schematic of the architecture, (b) energy level diagram (c) surface optical micrograph of P3HT:$PC_{61}BM$ active layer processed at 30sec, 60sec and 200sec.

3. Results and discussion

3.1. Crystallinity analysis of P3HT:$PC_{61}BM$

P3HT is a semi-crystalline conducting polymer and it crystallizes in monoclinic crystal system based on the processing method. The lamellar orientation and the crystalline domain size of P3HT depends on the film processing conditions, solvent use to prepare the solution preparation, molecular weight of the polymer and some extent surface treatment of the substrate. The crystalline properties also depends on the surrounding $PC_{61}BM$ acceptor in the P3HT:$PC_{61}BM$ mixture. Strength of P3HT $PC_{61}BM$ interaction influence the domain size of the P3HT in the mixture (Lilliu et al., 2011; Shen et al., 2016). For the high performance of organic solar cell, organic light emitting diode and photodiode requires high mobility in the orthogonal to the substrate direction. The charge carrier mobility is high along the P3HT backbone and conduction occurs by hopping from π-π stacking direction. By improving the crystallinity, the conductivity along the vertical direction can be improved. The thermal annealing of P3HT:$PC_{61}BM$ mixture crystallizes both P3HT and $PC_{61}BM$ individually. To achieve larger P3HT domain with nanoscale morphology is critical in the OPV fabrication. Fig. 2 shows the GIXRD pattern of P3HT:$PC_{61}BM$ active layer thin film processed at 30sec, 60sec and 200sec. Diffraction studies of samples were done using Rigaku diffractometer with X-ray wavelength of 1.541 Å. The XRD was done from the 2 theta angles from 2° to 30° with step size of 0.01°. The diffraction at 5.3° 2 theta angle corresponding to the (1 0 0) peak. The FWHM of 30sec, 60sec and 200 *sec* is 0.534, 0.461 and 0.493 respectively. Significant reduction in the FWHM and increase in the (0 0 1) peak intensity of P3HT implies that active layer processed with 60sec has larger *π-π* staking ordered domains. For the prepared P3HT and $PC_{61}BM$ ration and concentration, high crystallinity is observed for the spinning time of 60 *sec* and 140 °C. The crystalline done favors the charge carrier mobility and improve the optical absorption (Wie et al., 2014).

3.2. Raman and UV–Visible spectroscopy

Fig. 2 shows the measured Raman spectra for P3HT:$PC_{61}BM$ blend thin films. Raman spectra were recorded by using 514 nm LASER as light sources. The Raman peak at 1380 cm^{-1} and 1440–1450 cm^{-1} corresponds to the -C—C- skeletal stretching ($\nu_{C\text{-}C}$) and -C═C- symmetric stretching ($\nu_{C=C}$) respectively. Full width at half maximum (FWHM) value of -C═C- symmetric stretching of device A, device B and device C are 32.3 cm^{-1}, 31.4 cm^{-1} and 31.6 cm^{-1} respectively. Relative intensity of the device-A, device-B and device-C are 2212 counts, 2550 counts and 2420 counts respectively. Reduction in FWHM of C═C peak and intensity enhancement in symmetric stretching of C═C suggests that enhanced delocalization of *π*-electrons. C═C shifts to lower energies are infers increased *π*-electrons delocalization on C═C bonds between the fused-thiophene units and thiophene, infers a reduction in the inter unit bond dihedral angle between these units (Nalwa et al., 2011; Tsoi et al., 2011; Miller et al., 2008).

3.3. Mott-Schottky analysis

The capacitance–voltage study gives the information about the mid-gap states and the nature of depletion region formed in the semiconductor devices. Capacitance-voltage characteristic of devices is shown in the Fig. 3**(a)**. C-V study was carried out by setting perturbation *ac* voltage of 20 kHz and 0.01 V. Capacitance values are measured in the voltage range between −2V to 2 V with step size of 0.1 V. Applying small signal *ac* frequency activates trapped charge carriers. Detailed properties of the depletion nature of the devices was studied by Mott-Schottky analysis. The carrier concentration and bulit-in potential was obtained by Mott-Schottky study. Depends on the biasing condition either reverse bias (RB) or forward bias (FB) to the device. By studying the device at various biasing condition, one can evaluate the behavior depletion region. The Mott-Schottky relation (Carr and Chaudhary, 2013) is given in equation (1),

$$1/C^2 = \frac{2(V_{bi} - V)}{\varepsilon q N A^2} \quad (1)$$

where, A - contact area, ε- semiconductor permittivity, *N* - carrier concentration q - electronic charge, V_{bi} - built-in-potential. Under forward bias, slow decrease in capacitance is noted. Flat band condition is achieved when $V = V_{bi}$ due to the elimination of depletion region thereby diminishing the contribution of depletion capacitance giving rise to a maximum at V_{bi}. Under operational condition built-in voltage was calculated using Mott-Schottky characteristics and all the devices showed value of 540 mV. Calculated carrier concentration for device-A, device-B and device-C is 9.574 × 10^{16} cm^{-3}, 2.316 × 10^{16} cm^{-3} and 3.981 × 10^{16} cm^{-3}. The carrier accumulation progresses until the applied voltages reaches the peak voltage value (V_{peak}) then charge carrier overcomes the barrier and follows the continuous injection. As the charge carrier accumulation is high recombination rate is also high.

3.4. C-f and trap DOS analysis

Capacitance-frequency characteristic was measured to derive characteristics of the trap states in the device. C-f was done under dark condition at 0 V DC bias and it is shown in Fig. 3**(c)**. Capacitance values as a function frequency was measured from 1000 Hz to 10 MHz. Polymer solar cell offers capacitance is a strongly dependent on frequency. In lower frequency region, capacitance spreading occurs and as frequency increases towards the higher region, exponential decreases in capacitance dispersion occurs then saturates at sufficiently very higher frequency. Measured capacitance value in the lower end frequency at the 2 kHz device-A, device-B and device-C is 8.545 × 10^{-10} Fm^{-2}, 1.934 × 10^{-10} Fm^{-2} and 1.034 × 10^{-10} Fm^{-2} respectively. The device-B exhibits low density of trap states and this should be due to high crystallinity of the

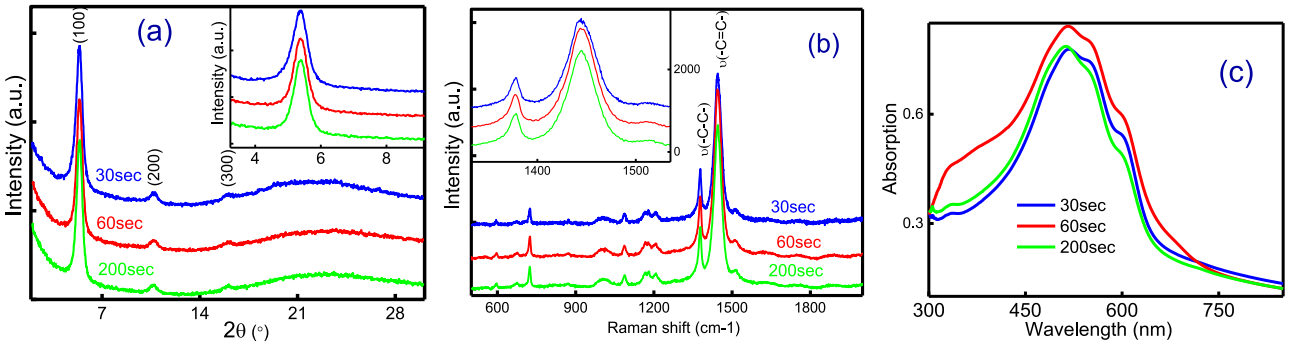

Fig. 2. (a) X-ray diffraction P3HT:$PC_{61}BM$ semiconductor, (b) Raman characteristics of semiconductor, and (c) UV–visible spectra of semiconductor.

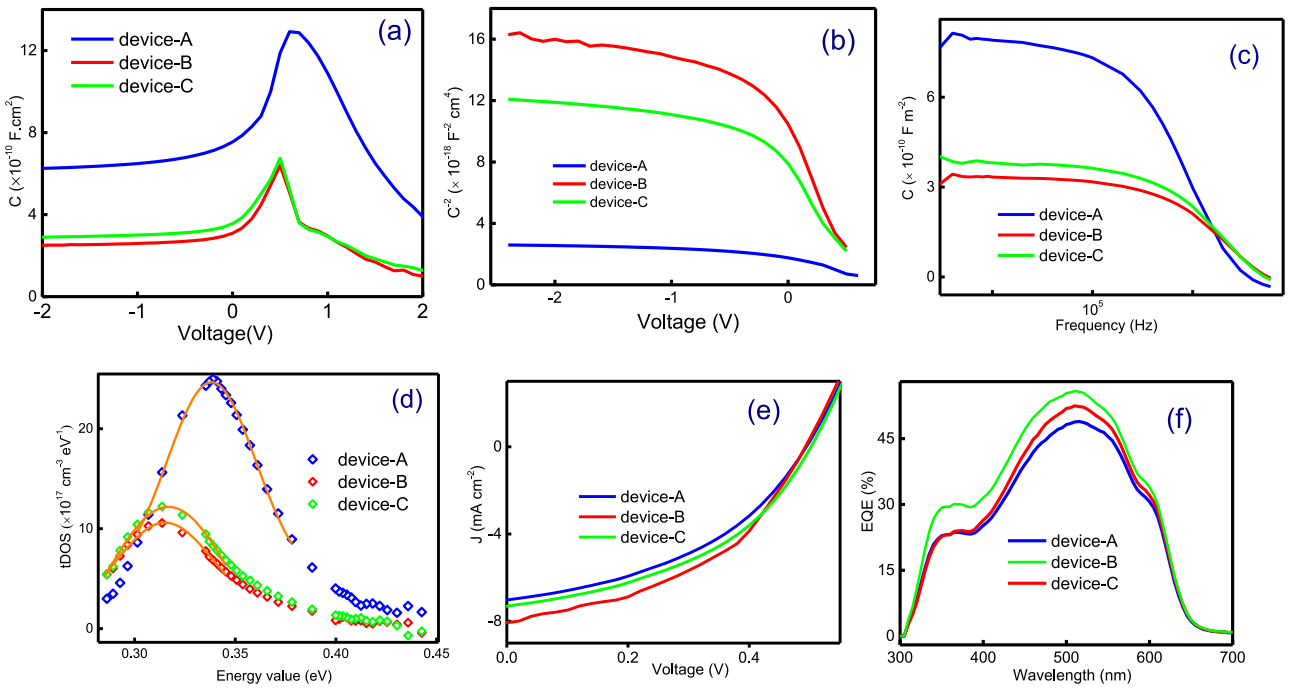

Fig. 3. (a) C-V plot, (b) Mott-Schottky characteristics, (c) *C-f* plot, (d) trap DOS plot, (e) solar cell characteristics and (f) external quantum efficiency spectra.

P3HT:$PC_{61}BM$ layer. Since, all the device processing parameter is same except the active layer spinning time, any change in the device properties should be due to the active layer contribution. Further, the trap properties were studied by C-f characteristics spectrum. Dynamics of the trapped charge trapped can characterized by attempt to escape frequency. In the low frequency region trap DOS can contribute to capacitance. However, under the perturbation of the ac small signal, the deeply trapped charge carrier can contributed capacitance. Without the perturbation frequency mostly shallow level trap can contribute to capacitance. Trap states near HOMO level of the polymer show high response at high frequencies and trapped charge which are far away from HOMO level will response slowly. The Trap DOS was studied based on the assumption of Gaussian distribution of states (Street et al., 2016).

$$N_T(E_\omega) = \frac{\beta}{qAd}\frac{V_{bi}}{kT}\frac{2f.dC}{d\omega} \quad (2)$$

$$E_\omega = kT.\ln(\omega_0/2f) \quad (3)$$

In the high frequency region all device capacitance falls into negative region. The device-A, device-B and device-C respectively exhibits the negative capacitance at the frequency of around 3.654 MHz, 5.205 MHz, 5.199 MHz. It is observed that negative capacitance falls off faster in device-A and device-C. Rapid fall of capacitance in the device-A and device-C should be due to one of the following reasons minority charge carrier t, interface trap states, slow transport time of interface carriers, trapped charges, space charge (Gommans et al., 2005). The distribution width of the trap states of device-A, device-B and device-C is 0.0484 eV, 0.0441 eV and 0.0682 eV respectively. The increase in the disorder states or marginally less crystallinity of the device-A and device-C active layer should be the cause of the increased trap state distribution width. To reduce the trap distribution width either crystallinity of the active layer can be improved or active layer should be optimized to attain the same. Trap distribution width maxima located at the energy value of 0.3382 eV, 0.3152 eV and 0.3169 eV respectively for device-A, device-B and device-C. The shifting of the trap energetic maxima towards the higher energy region indicates the trap location is moving towards the deep trap region end. This also indicates the increased number of deep trap states in the device. The total trap DOS is 1.109×10^{16} eV cm^{-3}, 5.879×10^{15} eV cm^{-3} and 7.696×10^{15} eV cm^{-3}.

Photovoltaics property of the devices are shown in the Fig. 3**(e)** and the quantum efficiency of the devices are shown in Fig. 3**(f)**. The short circuit current density of the devices-A, device-B and device-C are 7.256 mA cm^{-2}, 8.147 mA cm^{-2}, 7.511 mA cm^{-2} respectively. The open circuit voltage of the devices is 0.56 V and it is same for all the devices. Fill factor of the device is 45.9 %, 48.2 % and 47.2 % respectively for device-A, device-B and device-C. The efficiency of the device-B (2.202 %) is higher device-A (1.828 %) and device-C (1.981 %). Enhancement in the efficiency comes from the improvement J_{SC} and FF. J_{SC} enhancement in the device-B should be due to the high crystallinity of the active layer than device-A and device-C. The high percentage of the crystallinity of the active layer improve the optical absorption and also facilitates the charge carrier mobility. Enhancement in these two properties contributes to the J_{SC} improvement. Fill factor improvement should be due improvement in the series and shunt resistance of the device.

4. Conclusions

The effect of photoactive layer processing condition was studied. As the active layer spinning time changes the properties of the π-π stacking of the P3HT polymer changes and results in the change optoelectronic properties of the active layer. It is observed that spinning time changes the active layer properties drastically mainly the packing density of the crystalline region. The change in the crystalline nature of the semiconductor layer impact the photovoltaic properties. The crystallinity change in semiconductor layer also influences the shunt and series resistance. These resistance change alter the resultant J_{SC}. While the enhancement in the crystallinity contributes to enhanced optical absorption. The modification of the active layer properties through processing condition modifies the fill factor changes in the device-B shows that. It is noted that when the spinning time of the active layer changes optimized time, the crystallinity reduces. When deviating from the optimized spinning time the density of trap states also increase in the devices. The optoelectronic properties change of semiconductor is correlated with the crystallinity of the P3HT polymer. The result suggest that the crystallinity variation also modifies the total density of trap states.

Declaration of Competing Interest

The authors declare the following financial interests/personal relationships which may be considered as potential competing interests: This is partially supported by Science and Engineering Research Board, New Delhi, India. The grant number is SRG/2021/001690.

Data availability

Data will be made available on request.

Acknowledgment

This is partially supported by Science & Engineering Research Board, New Delhi, India. The grant number is SRG/2021/001690.

References

Carr, J.A., Chaudhary, S., 2013. The identification, characterization and mitigation of defect states in organic photovoltaic devices: A review and outlook. Energy Environ. Sci. 6 (12), 3414.

Gommans, H.H.P., Kemerink, M., Janssen, R.A.J., 2005. Negative capacitances in low-mobility solids. Phys. Rev. B - Condens. Matter Mater. Phys. 72 (23) https://doi.org/10.1103/PhysRevB.72.235204.

Kesavan, A.V., Jagdish, A.K., Ramamurthy, P.C., 2017. Light trapping and management in inverted organic solar cells employing metal nanoparticles. In: 2017 IEEE 44th Photovolt. Spec. Conf. PVSC 2017, p. 2017. https://doi.org/10.1109/PVSC.2017.8366818.

Kesavan, A.V., Adiga, V., Chandrasekar, G.K., Panidhara, K.M., Ramamurthy, P.C., 2022. Nanoscale small molecule self-assembled ITO for photon harvesting in polymer and perovskite solar cells. Sol. Energy. 240, 201–210. https://doi.org/10.1016/J.SOLENER.2022.05.002.

Kesavan, A.V., Ramamurthy, P.C., 2017. Source materials grain size effect on electrode microstructure and its effect on conventional bulk hetero-junction photovoltaics. Sol. Energy Mater. Sol. Cells. 172, 244–251. https://doi.org/10.1016/j.solmat.2017.07.044.

Kesavan, A.V., Khanum, K.K., Subbiahraj, S., Ramamurthy, P.C., 2019. Evaluation of polymer solar cell efficiency to understand the burn-in loss. J. Phys. Chem. C. 123, 22699–22705. https://doi.org/10.1021/ACS.JPCC.9B02584.

Koo, D., Jung, S., Oh, N.K., Choi, Y., Seo, J., Lee, J., Kim, U., Park, H., 2018. Improved charge transport via WSe 2 -mediated hole transporting layer toward efficient organic solar cells. Semicond. Sci. Technol. 33 (12), 125020.

Lilliu, S., Agostinelli, T., Pires, E., Hampton, M., Nelson, J., Macdonald, J.E., 2011. Dynamics of crystallization and disorder during annealing of P3HT/PCBM bulk heterojunctions. Macromolecules. 44 (8), 2725–2734.

Liu, Q., Jiang, Y., Jin, K., Qin, J., Xu, J., Li, W., Xiong, J., Liu, J., Xiao, Z., Sun, K., Yang, S., Zhang, X., Ding, L., 2020. 18% Efficiency organic solar cells. Sci. Bull. 65, 272–275. https://doi.org/10.1016/j.scib.2020.01.001.

Lu, L., Yu, L., 2014. Understanding low bandgap polymer PTB7 and optimizing polymer solar cells based on IT. Adv. Mater. 26, 4413–4430. https://doi.org/10.1002/adma.201400384.

Miller, S., Fanchini, G., Lin, Y.-Y., Li, C., Chen, C.-W., Su, W.-F., Chhowalla, M., 2008. Investigation of nanoscale morphological changes in organic photovoltaics during solvent vapor annealing. J. Mater. Chem. 18 (3), 306–312.

Nalwa, K.S., Mahadevapuram, R.C., Chaudhary, S., 2011. Growth rate dependent trap density in polythiophene-fullerene solar cells and its implications. Appl. Phys. Lett. 98 (9) https://doi.org/10.1063/1.3560483.

Nellissery Viswanathan, V., Ramamurthy, P.C., Varman, A.K., 2022. Enhancement in the Inherent Photostability of Small Molecule-Based Bhj Device by Molecular Architecturing. SSRN Electron. J. https://doi.org/10.2139/ssrn.4017230.

Rao, A.D., Murali, M.G., Kesavan, A.V., Ramamurthy, P.C., 2018. Experimental investigation of charge transfer, charge extraction, and charge carrier concentration in P3HT:PBD-DT-DPP:PC70BM ternary blend photovoltaics. Sol. Energy. 174, 1078–1084. https://doi.org/10.1016/j.solener.2018.09.072.

Shen, X., Hu, W., Russell, T.P., 2016. Measuring the degree of crystallinity in semicrystalline regioregular poly(3-hexylthiophene). Macromolecules. 49, 4501–4509. https://doi.org/10.1021/acs.macromol.6b00799.

Street, R.A., Yang, Y., Thompson, B.C., McCulloch, I., 2016. Capacitance spectroscopy of light induced trap states in organic solar cells. J. Phys. Chem. C. 120, 22169–22178. https://doi.org/10.1021/acs.jpcc.6b06561.

Sun, C., Qin, S., Wang, R., Chen, S., Pan, F., Qiu, B., Shang, Z., Meng, L., Zhang, C., Xiao, M., Yang, C., Li, Y., 2020. High efficiency polymer solar cells with efficient hole transfer at zero highest occupied molecular orbital offset between methylated polymer donor and brominated acceptor. J. Am. Chem. Soc. 142, 1465–1474. https://doi.org/10.1021/jacs.9b09939.

Tsoi, W.C., James, D.T., Kim, J.S., Nicholson, P.G., Murphy, C.E., Bradley, D.D.C., Nelson, J., Kim, J.-S., 2011. The nature of in-plane skeleton Raman modes of P3HT and their correlation to the degree of molecular order in P3HT:PCBM blend thin films. J. Am. Chem. Soc. 133 (25), 9834–9843.

Wie, J.J., Nguyen, N.A., Cwalina, C.D., Liu, J., Martin, D.C., Mackay, M.E., 2014. Shear-induced solution crystallization of poly(3-hexylthiophene) (P3HT). Macromolecules. 47 (10), 3343–3349.

Zhang, T., Dement, D.B., Ferry, V.E., Holmes, R.J., 2019. Intrinsic measurements of exciton transport in photovoltaic cells. Nat. Commun. 10, 1–10. https://doi.org/10.1038/s41467-019-09062-8.